Korean J. Chem. Eng., **31**(8), 1438-1443 (2014)
DOI: 10.1007/s11814-014-0060-0

pISSN: 0256-1115
eISSN: 1975-7220

Effect of polymer and additive on the structure and property of porous stainless steel hollow fiber

Xiao-Hua Ma, Yu Bai, Yue Cao, and Zhen-Liang Xu†

State Key Laboratory of Chemical Engineering, Membrane Science and Engineering R&D Lab.,
Chemical Engineering Research Center, East China University of Science and Technology,
130 Meilong Road, Shanghai 200237, China
(*Received 18 August 2013 • accepted 21 February 2014*)

Abstract−Porous stainless steel hollow fiber has been widely used due to its high mechanical strength, excellent thermal conductivity and good sealing properties compared with other porous supports. We successfully prepared porous stainless steel hollow fibers using polyacrylonitrile (PAN) as polymer via dry-wet spinning followed by sintering through temperature programming method. The PAN concentration had an obvious impact on the structure and property of porous stainless steel hollow fiber even if it would be burned off during sintering. The results showed that the morphology could be tuned by adjusting the concentration of PAN. With increasing PAN concentration in casting solution for spinning, the viscosity was increased dramatically, resulting in much compact structures with high pure water flux (higher than 3×10^5 $L\cdot m^{-2}\cdot h^{-1}\cdot Pa^{-1}$). A more dense structure could be obtained by adding additive polyvinylpyrrolidone (PVP) as viscosity enhancer.

Keywords: Porous Stainless Steel Hollow Fiber, Structure, Property, Polymer Concentration

INTRODUCTION

Stainless steel (316L) with good corrosion resistance, mechanical properties (excellent corrosion resistance, especially the pitting corrosion resistance, and high strength under high temperature) and low cost is widely used in the pulp and paper industry [1], chemical industry [2-4], food industry [5,6], water treatment and other fields [7]. Stainless steel membranes have been targeted for potential applications as porous supporting, composite membranes [8-10], fuel cell bipolar plates [1,11-13] and membrane reactors [14-16] for separation applications. For example, palladium membranes possess the ability to separate hydrogen exclusively from other gases. However, the use of pure palladium membranes for the hydrogen separation is restricted due to hydrogen embrittlement, which is still a very important and active topic in metal science. It is caused by the transition between the α- and β-phases occurring in membranes in contact with hydrogen at temperatures below 300 °C and pressures below 2 MPa [17]. Although hydrogen embrittlement can be reduced by alloying palladium with metals such as silver, nickel and copper [17] in the preparation process of composite palladium-based membranes (alloy membranes), the key to obtaining a membrane with high flux is a composite-type structure composed of a thin selective layer deposited onto a porous supports. Using composite palladium-based membranes (alloy membranes) with thin top layer instead of conventional thick walled tubes is more attractive due to the high hydrogen permeability [18]. Therefore, porous supports with good mechanical and thermal stabilities are of great importance and required to be produced easily and economically. Among the porous supports like glass, ceramic, and other metals in porous form, porous stainless steel might be a good choice due to its similar thermal expansion coefficient to the palladium-based films, ease of fabrication and processing, resistance to corrosion and crack. In addition, glass and ceramic supports tend to crack and break and are difficult to seal with permeation cell.

Up to now, there has been little report on the preparation of porous stainless steel hollow fiber. Luiten-Olieman et al. reported that the morphology of porous stainless steel hollow fibers could be tuned by controlling the stainless steel particle loading and the water concentration of the spinning solution [19]. And then they prepared porous stainless steel hollow fibers with shrinkage-controlled small radial dimensions (~250 μm) by controlling shrinkage during thermal treatment [20]. The polymer concentration also affected the structure and property of porous stainless steel hollow fiber, even if it was burned off during sintering. We used polyacrylonitrile (PAN) as polymer to prepare casting solution for spinning. To obtain a densified microstructure, the sintering temperature was 1,300 °C, much higher than that reported by Luiten-Olieman (1,100 °C) [19]. The effect of PAN concentration on the morphology and property of porous stainless steel hollow fiber was investigated by SEM, porosity, pore size, pure water flux, mechanical property, etc.

EXPERIMENTAL AND METHODS

1. Materials and Instrumentals

Polyacrylonitrile (PAN) was purchased from Jilin Jida Polymer Material Co., Ltd. (China). 316L stainless steel powders (400 mesh) were purchased from Zhejiang Haining Feida Metallurgical Powder Co., Ltd. (China). H_2 (99.5%) and N_2 (99.9%) were purchased from Shanghai Five-Steel Gas Co., Ltd. (China). All other solvents and reagents were analytical grade and purchased from Sinopharm Chemical Reagent Co. Ltd. De-ionized water was used throughout the study.

†To whom correspondence should be addressed.
E-mail: chemxuzl@ecust.edu.cn

2. Preparation of Membranes

PAN and 316L stainless steel powders (400 mesh) were dried under vacuum at 60 °C for 48 h before use. PAN was dissolved in 1-methyl-2-pyrrolidinone at 70 °C to obtain a homogeneous solution with PAN concentration of 6, 7, 8, 9 and 10 wt%, which were labeled as PAN6, PAN7, PAN8, PAN9 and PAN10. The concentration of the 316L stainless steel powders (400 mesh) was fixed at 50 wt%. The mixture was constantly stirred for 24 h to obtain a casting solution for spinning. Another group of casting solutions with 0.5 wt% additive polyvinylpyrrolidone (PVP) as viscosity enhancer was also prepared for spinning.

Stainless steel hollow fibers were spun by dry-wet spinning method, and the details were described elsewhere [21-23]. All spinning experiments were carried out at room temperature, and an overview of the spinning conditions are described in Table 1.

After being spun, the fabricated hollow fibers were kept in a deionized water bath for 24 h to remove the residual solvents before being dried in air at room temperature. The dried fibers were sintered by temperature programming method (average heating rate 5 °C/min) in a mixture gas atmosphere (75% H_2+25% N_2), as shown in Fig. 1.

3. Characterization

The viscosities of casting solutions with different PAN concentrations were investigated by a DV-II+PRO Digital Viscometer (Brookfield, USA) at 25 °C. The decomposition temperature of polymer was evaluated by thermogravimetric analysis (TGA) (TA SDT-Q600, USA). The TGA measurements were carried out under N_2 atmosphere at a heating rate of 5 °C/min from 0 °C to 1,000 °C. The morphologies of the hollow fibers were characterized by scanning electron microscope (SEM; JSM-6360LV, Japan).

Table 1. Spinning conditions

Condition	Value
Spinning mixture vessel temperature (°C)	50
Bore liquid	De-ionized water
External coagulant	De-ionized water
Mixture extrusion pressure (bar)	Corresponding to the mixture viscosity
Air gap (cm)	0
Bore liquid flow rate (ml/min)	9.99
Spinneret diameter (mm)	Outside diameter/ Inside diameter=1.5/1.0
Room temperature (°C)	25
Relative humidity (%)	38

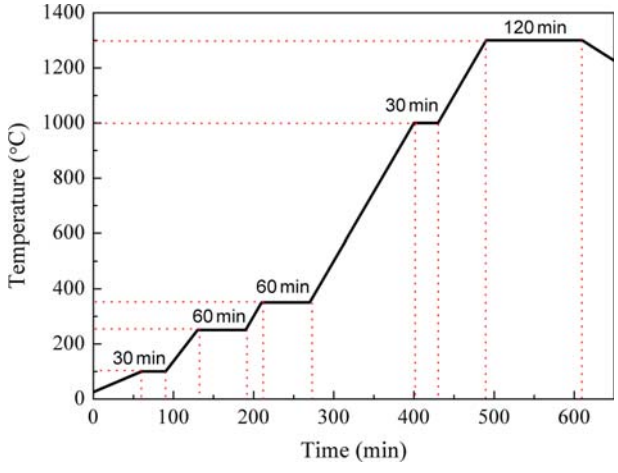

Fig. 1. Sintering program of green compact.

4. Fiber Density and Porosity Measurement

The fiber samples were dried under vacuum above 100 °C until a constant weight in dry state was achieved. The density of stainless steel hollow fibers before and after sintering could be calculated according to the definition of density as follows:

$$V = \frac{\pi L(D^2 - d^2)}{4} \tag{1}$$

$$\rho = \frac{m_1}{V} \tag{2}$$

where ρ is defined as the density (g/m^3); V is the volume (m^3); L, D, d and m_1 are the effective length (m), outside diameter (m), inside diameter (m) and dry weight (g) of the stainless steel hollow fibers, respectively.

The porosity ε(%) was defined as the volume of the pores divided by the total volume of the fiber. It could usually be determined by gravimetric method, based on the weight of liquid water contained in the fiber pores, as shown in Eq. (3):

$$\varepsilon = \frac{(m_2 - m_1)/\rho_w}{V} \tag{3}$$

where m_2 is the weight of wet fiber (g); and ρ_w is the water density (0.998 g/cm^3).

5. Maximum Pore Size Test

Maximum pore size D_{max} could be obtained by bubble point method. According to Laplace's equation, maximum pore size could be calculated:

$$D_{max} = \frac{4\sigma\cos\theta}{P} \tag{4}$$

where σ is the surface tension of water (72.25×10^{-3} N·m^{-1}); θ is the contact angle of water to membrane (°); and P is the minimum bubble point pressure (Pa).

6. Permeation Property Test

The permeation property was characterized by pure water flux (PWF). The PWF was measured using a dead-end flowing cell connected to compressed air as the feeding pressure, the detail of which was exhibited in our earlier work [24]. The filtration experiments were at room temperature and the hollow fiber membranes were pre-pressed at 0.1 MPa (1.0 bar) using pure water for 1 h before measurement, and PWF would be obtained by Eq. (5):

$$PWF = \frac{Q}{A\times t\times P} \tag{5}$$

where PWF is the permeation flux of membrane for pure water (L· m^{-2}·h^{-1}·bar^{-1}); Q is the volume of the permeated pure water (L); A is the effective area of the membrane (m^2), calculated by the average outside diameter of hollow fibers, as shown in Eq. (6), in which n is the number of fibers; t is the permeation time (h); and P is the operation pressure (=1.0 bar).

$$A=4\pi\times n\times D\times L \quad (6)$$

7. Mechanical Property Test

A universal testing machine (QJ210A, China) with a speed of 50 mm/min at room temperature was used to test the mechanical property of the green compact. The distance between two clips was 25 mm. The reported values were measured five times for each sample and then averaged.

After being sintered, the membrane was too brittle to be tested by the universal testing machine. A three-point bending test with a speed of 2 mm/min at room temperature was used to test the mechanical property of these fibers. The distance between two clips was 30 mm. The reported values were measured five times for each sample and then averaged.

RESULTS AND DISCUSSION

1. Effect of Viscosity on Spinning Process

The viscosities of casting solutions are shown in Fig. 2. With the increasing of PAN concentration, the viscosity of casting solution increases greatly due to the result of an increase in flow resistance (internal friction among stainless steel powders and external friction between stainless steel powders and PAN). In particular, the viscosity of casting solution determines the exchanging rate of solvent and non-solvent during phase inversion, further affecting the microstructure and property of the fiber. Our experiment showed that hollow fiber could not be fabricated when the casting solution for spinning contained 10 wt% PAN because the viscosity was too high. And the casting solution with 8 wt% PAN (~10,000 mPa·s) was suitable for spinning fibers with good morphologies and microstructures.

2. Decomposition Temperature of Polymer

The stainless steel hollow fiber was finally obtained after polymers has been burned off by sintering. To determine the sintering temperature, the thermal stability of the green compact was measured by means of TGA and the result is shown in Fig. 3. It can be seen that the starting point of weight loss begins at 60 °C (possibly due to the evaporation of water) and reaches the highest slope at around 200 °C (possibly due to the decomposition of the polymer). From the deriv. weight curve, three obvious peaks are observed at 75 °C, 214 °C and 305 °C, respectively, agreeing well with the weight loss

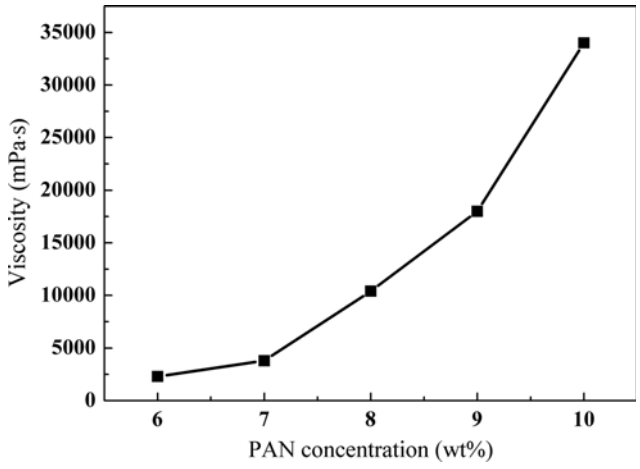

Fig. 2. Viscosity of casting solution for spinning.

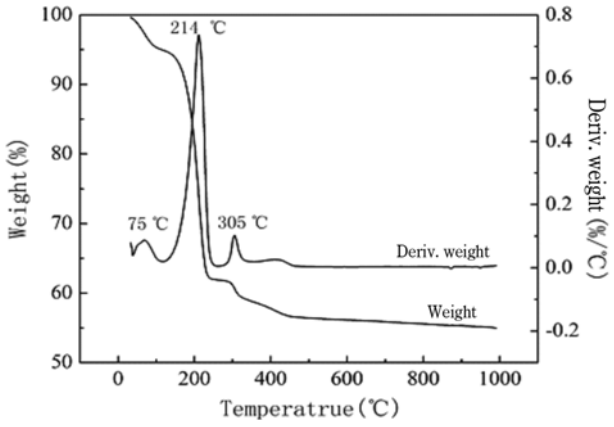

Fig. 3. TGA curves of green compact with 9 wt% PAN and 0.5 wt% PVP.

curve. The first small peak at 75 °C is attributed to the evaporation of water and part of solvent. The second obvious peak at 214 °C is related to the decomposition of PAN. And the third small peak at 305 °C corresponds to the decomposition of PVP since the decomposition temperature of PVP with a ring structure should be slightly higher than that of PAN with a chain structure. It can be reasonably deduced that the polymer begins to decomposition at 200 °C under N_2 atmosphere.

3. Morphologies

SEM is an effective way to present the morphologies of stainless steel hollow fiber before and after sintering. Fibers on the left are the green compact, while fibers on the right are their sintered counterpart at 1,300 °C. It is obvious that the PAN concentration has a significant influence on the morphology of the derived hollow fiber. The green compacts in Fig. 4 illustrate that near the outer and inner walls of the green compact, finger-like structures are obtained and at the center, there are sponge-like structures. The former can be attributed to the rapid precipitation occurring at both inner and outer fiber walls, while the latter sponge-like structure is ascribed to the slow precipitation taking place at the center of the fiber. The cross-section of hollow fiber reveals macrovoids (finger-like voids). With the increase of PAN concentration, a decrease in the size of macrovoids is observed mainly due to the reduction in the amount of nonsolvent (water) required to induce phase separation of a spinning mixture. It is well known that for spinning mixtures with a composition closer to the phase boundary, more regular structure will be obtained (sponge-like structure) with less and smaller voids [19]. Another nonsolvent instead of water could be used as bore liquid and/or external coagulant to reduce macrovoids by decreasing transfer rate between nonsolvent and solvent.

Although macrovoids still can be observed after being sintered, they are smaller and fewer in number (Fig. 4b, d, f, h), which is similar to the results of Luiten-Olieman [19] et al. for porous stainless steel hollow fiber. A moderate shrinkage during the heat treatment was observed. According to Luiten-Olieman and Kuiken [19,25], during viscous sintering, the macrovoid volume in the fiber is reduced, causing shrinkage of the fiber (Fig. 4). When the particle loading is too high, the viscoelastic properties of the green fiber are dictated by the particles rather than the polymer, and viscous deformation is observed. The viscous deformation is driven by a reduction in surface

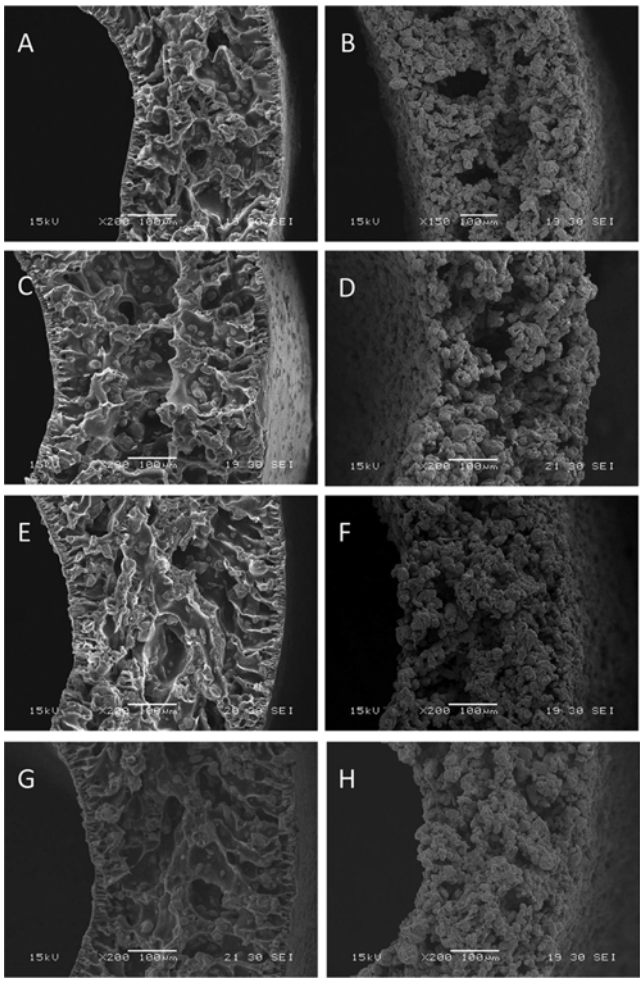

Fig. 4. SEM cross-section image of stainless steel hollow fiber with 6-9% PAN (A): PAN6 green compact, (B): PAN6 sintered 1,300 °C, (C): PAN7 green compact, (D): PAN7 sintered 1,300 °C, (E): PAN8 green compact, (F): PAN8 sintered 1,300 °C, (G): PAN9 green compact, (H): PAN9 sintered 1,300 °C.

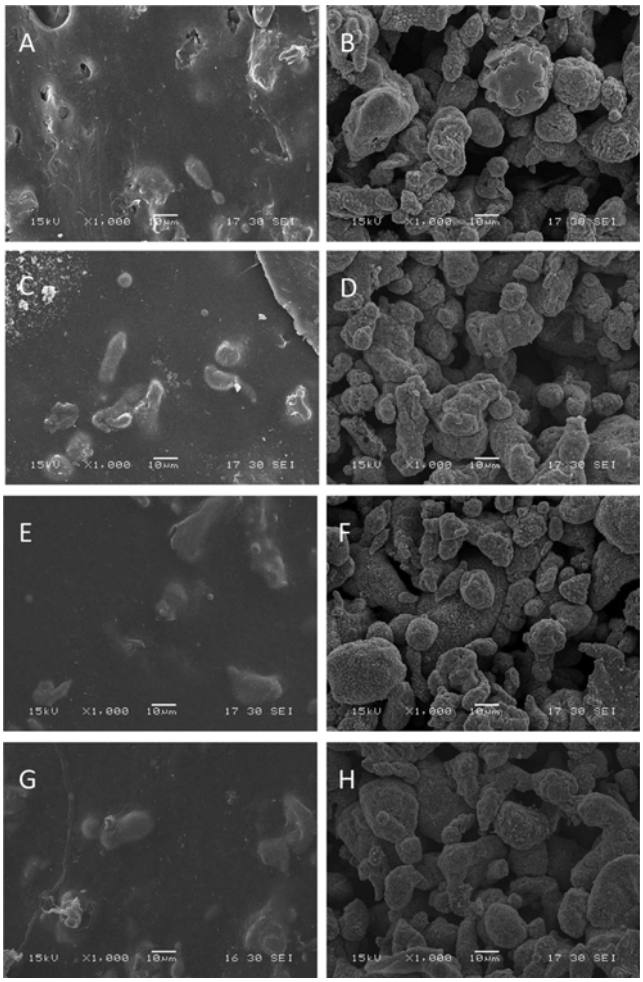

Fig. 5. SEM outside surface image of stainless steel hollow fiber with 6-9% PAN (A): PAN6 green compact, (B): PAN6 sintered 1,300 °C, (C): PAN7 green compact, (D): PAN7 sintered 1,300 °C, (E): PAN8 green compact, (F): PAN8 sintered 1,300 °C, (G): PAN9 green compact, (H): PAN9 sintered 1,300 °C.

free energy associated with the macrovoids, and the shape and size of these macrovoids are expected to have an influence on the rate of macrovoid decay.

The outside surface images of stainless steel hollow fibers before and after sintering are shown in Fig. 5. The surface of the green compact is similar to that of the conventional polymeric membrane prepared via the phase-inversion technique. After thermal treatment, the surface structure becomes coarse and porous, revealing that the

Table 2. Density and porosity of stainless steel hollow fiber

Item	Green compact		Sintered 1,300 °C					
	Density ($g \cdot cm^{-3}$)	Porosity (%)	Density ($g \cdot cm^{-3}$)	Porosity (%)	Bubble point pressure (MPa)	Maximum pore size (μm)	Main pore size (μm)	PWF ($10^5\ L \cdot m^{-2} \cdot h^{-1} \cdot Pa^{-1}$)
PAN6	1.00	43	1.61	51	0.0074	39.2	21.4	26.1
PAN7	1.00	35	1.79	48	0.0078	36.9	18.6	15.3
PAN8	1.03	33	2.06	45	0.0106	27.3	16.8	9.20
PAN9	1.25	30	2.09	44	0.0108	26.7	15.3	6.54
PAN6-PVP0.5	1.02	50	1.73	48	0.0085	34.0	19.7	16.9
PAN7-PVP0.5	1.13	47	1.98	46	0.0096	30.1	17.5	8.99
PAN8-PVP0.5	1.17	45	2.17	44	0.0111	26.0	15.9	5.45
PAN9-PVP0.5	1.41	38	2.39	43	0.0117	24.6	14.1	3.16

Table 3. Mechanical properties of stainless steel hollow fiber

Item	Green compact			Sintered 1,300 °C	
	Break strength (MPa)	Elongation at break (%)	Young's modulus (MPa)	Break strength (MPa)	Flexural modulus (MPa)
PAN6	2.21	4.0	38.2	3.30	1765
PAN7	2.63	6.0	43.4	3.95	2738
PAN8	3.32	7.0	66.6	5.46	3554
PAN9	3.88	11	83.4	6.69	3872
PAN6-PVP0.5	2.22	4.0	43.7	3.87	2404
PAN7-PVP0.5	2.54	5.0	57.4	4.64	2944
PAN8-PVP0.5	3.85	8.0	70.5	5.94	3753
PAN9-PVP0.5	4.22	11	90.4	7.12	3906

polymer has been burned off completely.

4. Density, Porosity, Bubble Point, Maximum Pore Size and Pure Water Flux

To investigate the influence of PAN concentration on the structure and property of the hollow fiber before and after sintering, density, porosity, bubble point, maximum pore size and pure water flux are tested and the results are shown in Table 2. With increasing PAN concentration, the densities of both hollow fiber before and after sintering increase and the porosities both decrease. After PAN is burned off, the resulting fiber shrinks, leading to increasing density and porosity compared with green compact. Furthermore, the maximum pore size (likely the defect pores) and main pore size (14.1-21.4 μm) decrease and the bubble point pressure increases with increasing PAN concentration. The results indicate that the higher the PAN concentration, the denser membrane is to be expected.

The results of permeation property tested by PWF are also shown in Table 2. With increasing PAN concentration, the PWF decreases due to the more compact structure, but all the values are higher than 3×10^5 L·m^{-2}·h^{-1}·Pa^{-1}.

5. Mechanical Property

To verify whether the obtained stainless steel hollow fiber has outstanding mechanical strength, thermal shock resistance, and allows for welding or brazing, the mechanical property is measured and the results are shown in Table 3. With increasing PAN concentration in spinning mixture, the break strength, elongation at break and Young's modulus of green compact show a large increase due to the great density, dense structure as well as tight molecule tangle. After sintering at 1,300 °C, the flexural modulus displays an apparent increase due to the densification of structure.

6. Effect of Additive

To investigate the effect of viscosity on the structure and property of stainless steel hollow fiber, PVP was added into the casting solution as viscosity enhancer. During the experiment, it was observed that the viscosity increased when adding 0.5 wt% PVP as viscosity enhancer. Fig. 6 shows SEM cross-section image of stainless steel hollow fiber with 6.0-9.0 wt% PAN and 0.5 wt% PVP. It is notable that some macrovoids still exist in the SEM images (Fig. 4). However, a more dense structure as well as smaller voids was observed, resulting in high density and bubble point pressure as well as low maximum pore size and PWF (Table 2). This is probably advantageous for preparing stainless steel hollow fiber with small pore size because polymer will be finally burned off completely.

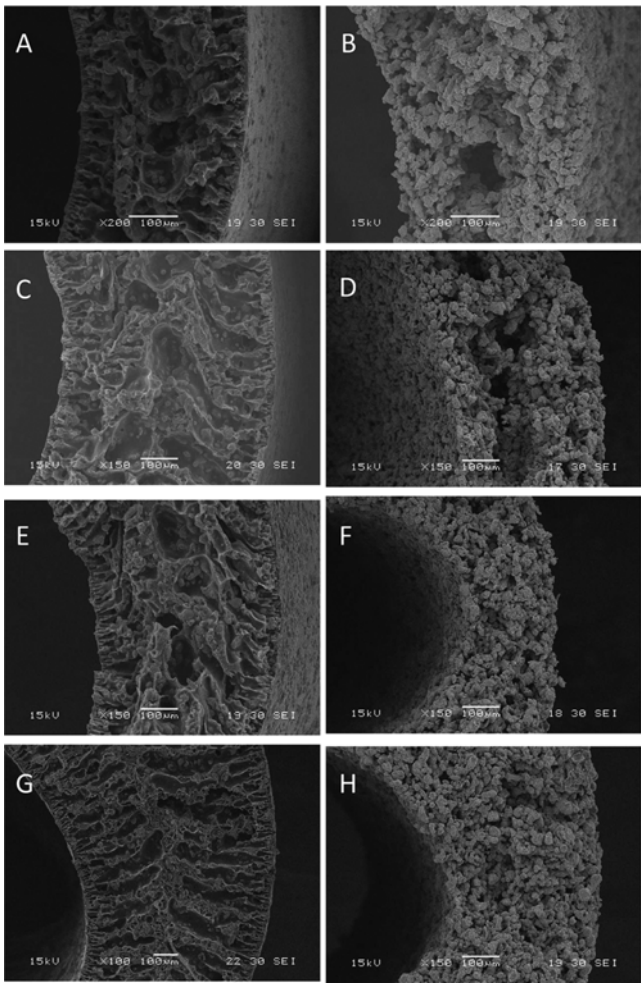

Fig. 6. SEM cross-section image of stainless steel hollow fiber with 6-9% PAN and 0.5% PVP (A): PAN6-PVP0.5 green compact, (B): PAN6-PVP0.5 sintered 1,300 °C, (C): PAN7-PVP0.5 green compact, (D): PAN7-PVP0.5 sintered 1,300 °C, (E): PAN8-PVP0.5 green compact, (F): PAN8-PVP0.5 sintered 1,300 °C, (G): PAN9-PVP0.5 green compact, (H): PAN9-PVP0.5 sintered 1,300 °C.

The outside surface SEM image of stainless steel hollow fibers containing 0.5 wt% PVP (Fig. 7) is also similar to that without PVP (Fig. 5), still advantageous for the mechanical property (Table 3).

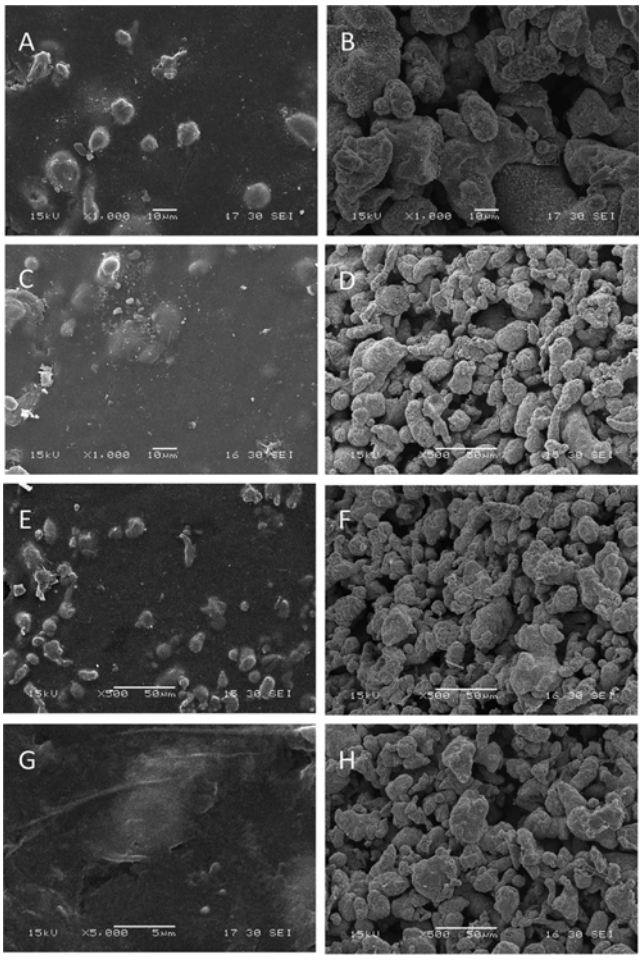

Fig. 7. SEM outside surface image of stainless steel hollow fiber with 6-9% PAN and 0.5% PVP (A): PAN6-PVP0.5 green compact, (B): PAN6-PVP0.5 sintered 1,300 °C, (C): PAN7-PVP0.5 green compact, (D): PAN7-PVP0.5 sintered 1,300 °C, (E): PAN8-PVP0.5 green compact, (F): PAN8-PVP0.5 sintered 1,300 °C, (G): PAN9-PVP0.5 green compact, (H): PAN9-PVP0.5 sintered 1,300 °C.

CONCLUSIONS

Porous 316L stainless steel hollow fibers were successfully prepared via dry-wet spinning and followed by sintering. All of the stainless steel fibers had sponge-like structures after sintering, even the green compacts with finger-like structures and some macrovoids. The microstructure of the obtained fibers could be tuned by adjusting PAN concentration. With increasing PAN concentration in the casting solution for spinning, the viscosity was increased dramatically, resulting in more compact structures but still with high pure water permeability (higher than 3×10^5 $L\cdot m^{-2}\cdot h^{-1}\cdot Pa^{-1}$). The results showed that casting solution with 8 wt% PAN (~10,000 mPa·s) was suitable for spinning fibers with good morphologies and microstructures. A more dense structure of stainless steel hollow fiber would be obtained by adding additive PVP.

ACKNOWLEDGEMENTS

The authors gratefully acknowledge Yang-fan Project for Young Talents of Science and Technology from Shanghai Committee of Science and Technology in China (14YF1404800), the Fundamental Research Funds for the Central Universities (WA1214062), the First-class General Financial Grant from the China Postdoctoral Science Foundation (2013M540336) and the National Natural Science Foundation of China (20076009, 21176067 and 21276075) for giving financial support.

REFERENCES

1. M. Senatore, L. Finzetto and E. Perea, *Rem-Revista Escola De Minas*, **60**, 175 (2007).
2. R. Sangeetha, R. Kumar, M. Doble and R. Venkatesan, *Colloids Surf. B-Biointerfaces*, **79**, 524 (2010).
3. S. Trigwell and G. Selvaduray, *J. Mater. Process. Technol.*, **166**, 30 (2005).
4. J. C. Stinville, P. Villechaise, C. Templier, J. P. Riviere and M. Drouet, *Surf. Coat. Technol.*, **204**, 1947 (2010).
5. L. Ceschini, C. Chiavari, E. Lanzoni and C. Martini, *Mater. Design*, **38**, 154 (2012).
6. P. M. D. Silva, H. F. G. de Abreu, V. H. C. de Albuquerque, P. D. Neto and J. Tavares, *Mater. Design*, **32**, 605 (2011).
7. T. M. Sridhar, U. Kamachi Mudali and M. Subbaiyan, *Corros. Sci.*, **45**, 237 (2003).
8. J. A. Calles, R. Sanz and D. Alique, *Int. J. Hydrogen Energy*, **37**, 6030 (2012).
9. M. L. Bosko, J. F. Munera, E. A. Lombardo and L. M. Cornaglia, *J. Membr. Sci.*, **364**, 17 (2010).
10. T. A. Peters, W. M. Tucho, A. Ramachandran, M. Stange, J. C. Walmsley, R. Holmestad, A. Borg and R. Bredesen, *J. Membr. Sci.*, **326**, 572 (2009).
11. H. L. Wang, M. A. Sweikart and J. A. Turner, *J. Power Sources*, **115**, 243 (2003).
12. Y. Wang and D. O. Northwood, *J. Power Sources*, **165**, 293 (2007).
13. Y. Fu, G. Q. Lin, M. Hou, B. Wu, Z. G. Shao and B. L. Yi, *Int. J. Hydrogen Energy*, **34**, 405 (2009).
14. A. Brunetti, G. Barbieri, E. Drioli, K. H. Lee, B. Sea and D. W. Lee, *Chem. Eng. Process.*, **46**, 119 (2007).
15. A. Brunetti, G. Barbieri, E. Drioli, T. Granato and K.H. Lee, *Chem. Eng. Sci.*, **62**, 5621 (2007).
16. A. Basile, P. Pinacci, A. Iulianelli, M. Broglia, F. Drago, S. Liguori, T. Longo and V. Calabro, *Int. J. Hydrogen Energy*, **36**, 2029 (2011).
17. S.-E. Nam, S.-H. Lee and K.-H. Lee, *J. Membr. Sci.*, **153**, 163 (1999).
18. H. Gao, Y. S. Lin, Y. Li and B. Zhang, *Ind. Eng. Chem. Res.*, **43**, 6920 (2004).
19. M. W. J. Luiten-Olieman, L. Winnubst, A. Nijmeijer, M. Wessling and N. E. Benes, *J. Membr. Sci.*, **370**, 124 (2011).
20. M. W. J. Luiten-Olieman, M. J. T. Raaijmakers, L. Winnubst, M. Wessling, A. Nijmeijer and N. E. Benes, *Scripta Mater.*, **65**, 25 (2011).
21. L.-Y. Yu, Z.-L. Xu, H.-M. Shen and H. Yang, *J. Membr. Sci.*, **337**, 257 (2009).
22. T.-S. Chung and Z.-L. Xu, *J. Membr. Sci.*, **147**, 35 (1998).
23. S. P. Deshmukh and K. Li, *J. Membr. Sci.*, **150**, 75 (1998).
24. L.-F. Han, Z.-L. Xu, Y. Cao, Y.-M. Wei and H.-T. Xu, *J. Membr. Sci.*, **372**, 154 (2011).
25. H. K. Kuiken, *J. Fluid Mech.*, **214**, 503 (1990).